Yuzuncu Yil University
Journal of Agricultural Sciences

(Yüzüncü Yıl Üniversitesi Tarım Bilimleri Dergisi)

https://dergipark.org.tr/en/pub/yyutbd

Research Article

Determination of Separation Performance in CFD-DEM Simulation Using Straw Particles in A Standard Cyclone

Nuri ORHAN*[1], Seda ŞAHİN[2], Mehmet BAHADIR[3]

[1,2] University of Selcuk Department of Agricultural Machinery and Technologies Engineering Alaeddin Keykubat Campus, Konya, Turkey
[3] University of Selcuk, Çumra Vocational School, Vegetable and Animal Production Organic Farming, Çumra, Konya, Turkey

[1] https://orcid.org/0000-0002-9987-1695, [2] https://orcid.org/0000-0003-1743-9530, [3] https://orcid.org/0000-0002-5071-5085

*Corresponding author e-mail: nuriorhan@selcuk.edu.tr

Abstract: Although flow in biological materials sometimes behaves like a continuous one, it cannot be simulated with continuity-based modeling when it comes to discontinuous flow behavior. The Discrete Element Method (DEM) in combination with Computational Fluid Dynamics (CFD) is a computational method for modeling particles in fluid flow by tracking their motion. DEM is widely used in the field of engineering, and its use in the agricultural field is increasing. This study analyzes the CFD-DEM relationship of biological material in aerodynamic systems and reviews current applications. In the article, the definition of aerodynamic systems as a basic principle, particle-fluid and particle-particle interaction forces in the system, modeling of particle motions, CFD-DEM coupling method, and analysis applications of agricultural aerodynamic systems are examined. In this study, simulation experiments were carried out at 100 g/s and 200 g/s straw feeding values at each value of 18-15-12-10-8-6-4 m/s air and straw inlet velocities. The flow near the cyclone walls caused the straw particles to be directed towards the lower exit end of the cyclone. At feed densities of 100 g/s and 200 g/s, the least particle output was obtained at a rate of 18 m/s. The highest cyclone output efficiency was obtained at feed densities of 100 g/s and 200 g/s at a velocity of 12 m/s. The compatibility of the trial simulation results with the literature showed that the CFD-DEM application is an important approach to study the behavior of particulate matter in fluids.

1. Introduction

The cyclone separator in the agricultural processing industry is considered one of the simplest and least expensive pieces of equipment for gas particulate matter separation. But cyclones have a complex flow pattern. Traditionally, the cyclone has been widely used in various industrial applications due to its high efficiency, simple design, relatively low cost of maintenance, flexible structure, and low power consumption (Wang et al., 2002; Marinuc and Rus, 2011;). One of the widely preferred areas is its use in separation processes (Avcı and Erel, 2003).

Cyclones are designed tangentially or axially according to the inlet type. Generally, tangential inlets are more commonly used for separation in cyclones. The fluid entering the cyclone gains a rotational motion with the effect of inertial forces. This rotational motion causes the fluid to be affected by the vortex motion. A relative movement in the radial direction occurs under the effect of different inertia forces on phases with different densities in the fluid. Part of the dense phase is removed from the flow area by the effect of centrifugal force (Şendoğan, 2012).

The cyclone's input section, body length, discharge pipe diameter, fluid flow, and physical qualities of the material employed all have an impact on cyclone efficiency. For these parameters to work in harmony with each other, their values must be determined optimally. More experimental studies should be done to determine these values (Şendoğan, 2012).

There are two most important points in cyclone design and selection. These are efficiency and pressure loss. The most important factors affecting the efficiency of the cyclone are the rate of entry of the particles into the cyclone and the amount of particle feed.

Inlet velocity affects both efficiency and pressure drop. As a result, the velocity must be improved. Cyclone performance can be enhanced under non-specific conditions by employing high input velocities, but performance can be diminished by increasing cyclone diameter (Faulkner and Shaw, 2006). Especially in the optimization of cyclone-style separators where the design parameters are dependent on each other, the use of programs that work according to computational fluid dynamics models facilitates the design and optimization. The flow parameters of high eddy and turbulent fluids may be easily calculated using computational fluid dynamics (CFD) models (Chu et al., 2011). As a result, crucial information for forecasting the aerodynamic behavior of the cyclonic-style separation process may be gained. Recently, high-order turbulence models using the unstable Reynolds mean Navier-Stokes (RANS) formulation, such as the Reynolds Stress Model (RSM), have shown adequate numerical estimate capabilities (Jakirlic et al., 2002; Gronald and Derksen, 2011). Cortes and Gil (2007) conduct a thorough examination of numerical CFD turbulence models for cyclone separators, concluding that proper resolution of flow characteristics is required for a successful simulation. The inclusion of particle matter in the cyclone's air flow necessitates extra modeling computations. As a result, the best numerical approach is Cundall and Strack (1979)'s Discrete Element Method (DEM), which uses the Lagrangian formulation technique to monitor each particle matter in the system independently. One can accurately predict the particulate flow behavior by considering the fluid-particle contact fundamentals of particle-particle, particle-boundary, and Newton's laws of motion (Peng et al., 2020; Zhu et al., 2008; Chu et al., 2011) and can analyze all physical phenomena. A schematic flowchart is shown in Figure 1 (Peng et al., 2020; Zhou et al., 2020) to provide an overview of the DEM algorithm.

Today, agricultural products (wheat, barley, etc.) are generally harvested with a combine harvester, and the remaining straw is either made into bales or chaff is made with a straw shredder machine (thresher machine). In small lands where the combine does not enter, the straw and seed parts of agricultural products are separated by threshing machines with or without storage. In addition, the harvesting and threshing processes of legumes such as chickpeas and beans are also carried out with threshing machines, with or without storage. The straw coming out of these threshing machines needs to be loaded, transported, and stored. The bagging process is widely used in the transportation or storage of hay. The bagging process is costly in terms of labor and causes a lot of time loss.

This study aims to optimize the design of the cyclone (separator) part of the cyclone regular straw bagging system, for which a patent application has been made for the straw bagging process by using CFD and DEM methods. In this context, flow analysis and particulate flow (air-straw) analyses of the cyclone, designed according to the literature, were carried out at different air inlet velocities with CFD and DEM based programs. Time-dependent separation and cyclone yield analysis of straw at different air velocities and feeding conditions in the cyclone were performed with CFD ANSYS Fluent and ROCKY DEM software. In this context, simulation experiments were carried out at 100 g/s and 200 g/s straw feeding values at each value of 18-15-12-10-8-6-4 m/s air and straw inlet velocities.

Set up
Import geomerties-Set up particles group-
Desing the parameters of particle-particle and
particle-boundary

Processig
Locating the particles and boundaries that
will ve contacted-determination all force, F
acting on the particles using

$$\sum F = F_{contact} + F_{body} = ma$$

Movement
The current particles position, velocity, an time step
was used for the movement of the particles from one
position to another as following equations.

$$\Delta V = \int \frac{\Sigma F}{m} dt : V_{new} = V_{old} + \Delta V$$

$$\Delta X = \int \Delta V_{new} dt : X_{new} = X_{old} + \Delta X$$

Where V is the velocity, X is the particle position,
and dt is the time step.

Stop
Simulating
processing

No

Repeat
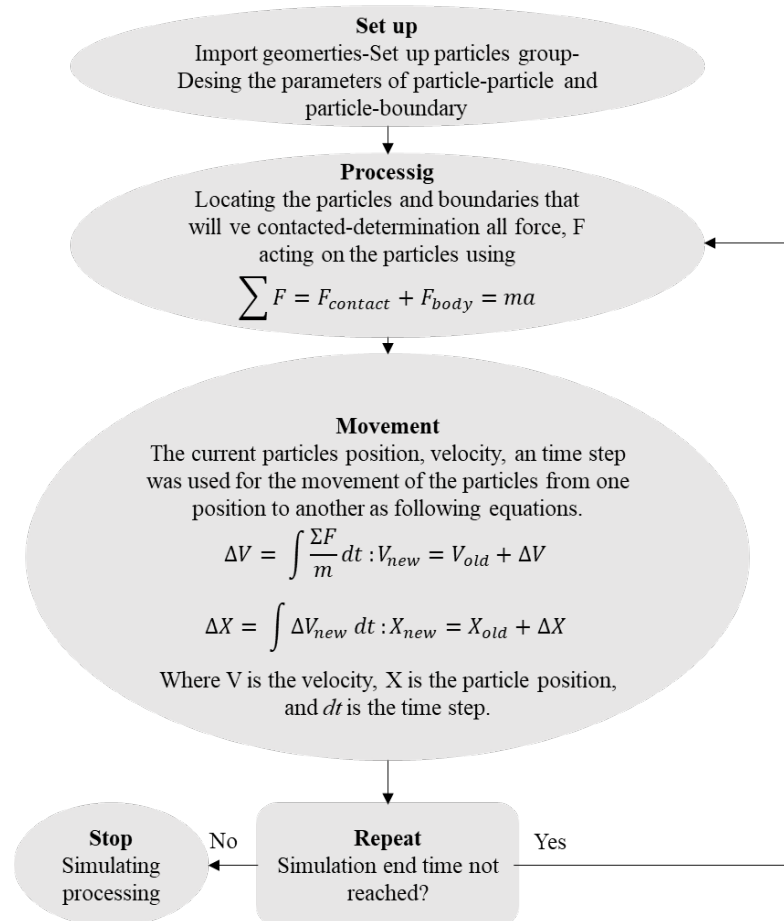Simulation end time not
reached?

Yes

Figure 1. Flowchart of the discrete element method.

2. Material and Method

The fluid phase motion is estimated using the Navier-Stokes equations in the continuous flow model, which divides the system area into tiny cells (Drew, 1983; Fluent, 2009; Neuwirth et al., 2013; Fonte et al., 2015; He et al., 2018). Fluid control in the cyclone is estimated in the CFD simulation using Equation (1-2) to determine continuity/conservation of mass and conservation of momentum, respectively. A finite volume approach was used to solve these equations using the CFD ANSYS-Release-19 software within Selçuk University.

$$\frac{\partial(\rho_f)}{d_t} + \nabla(\rho_f v_f) = 0 \tag{1}$$

$$\frac{\partial(\rho_f v_f)}{d_t} + \nabla(\rho_f v_f v_f) = -\nabla p + \nabla \tau_f + \rho_f g + \nabla(-\rho_f u_i' u_j') \tag{2}$$

Where ρ_f is the density of the fluid, t is the real-time, ∂t is indeed the difference in operators at period, v_f is the mean flow rate, p is the pressure, and τ_f is the viscous stress tensor of the fluid, g represents gravity, $u_i' u_j'$ represents the mean variable fluid velocity, and $\rho_f u_i' u_j'$ represents the Reynolds stress nonlinear component due to turbulence.

The Reynolds stress model (RSM) was adopted for the current investigation because of the severe eddies and anisotropic turbulence within the cyclone (Gimbun et al., 2005; Xiang and Lee, 2005; Wan et al., 2008; Gronald and Derksen, 2011; El-Emam et al., 2021).

The primary strategy to follow the particle phase trajectory in the area under examination is to use the Lagrangian method in DEM software (El-Emam et al., 2021). The motion of particulate matter is split into two categories: translational motion, which is defined by Newton's second law (Equation 3), and rotational motion, which is defined by Euler's law (Equation 4).

$$m_i \frac{du_i}{dt} = \sum_{j=1}^{n_i^c} F_{ij}^C + F_i^f + F_i^g \tag{3}$$

$$I_i \frac{d\omega_i}{dt} = \sum_{j=1}^{n_i^c} M_{ij} \tag{4}$$

Where m_i is the particle mass and u_i and ω_i are the particle i's translation and rotation velocities, respectively. The contact force and torque exerted on particle I by particle j or the wall, respectively, are F_{ij}^c and M_{ij}. F_i^f fluid-particle interaction forces, F_i^g gravitational force I_i is the second moment of particle i and t is time.

The Hysteretic Linear Spring Model (Walton and Braun, 1986) is utilized in this work to reduce the overhead of extensive simulation times. Because the velocities and charge rates of surrounding particles are ignored, the energy loss is unaffected by other connections. This model can also be due to repeated compressible materials incorporating non-adhesive particle flow. (Freireich et al., 2009; Fonte et al., 2015; Almeida et al., 2016). The DEM approach produced and employed the following Equation (5-8) to mathematically describe this model (Walton and Braun, 1986; Rocky, 2018).

$$F_i^{n,T} = \begin{cases} \min(F_i^{n,(T-\Delta T)} + K_u^n \Delta S^n, K_l^n S^{n,T}), & \text{if} \Delta S^n \geq 0 \\ \max(F_i^{n,(T-\Delta T)} + K_u^n \Delta S^n, 0.001\ K_l^n S^{n,T}), & \text{if} \Delta S^n < 0 \end{cases} \tag{5}$$

$$\Delta S^n = S^{n,T} - S^{n,T-\Delta T} \tag{6}$$

$$\frac{1}{K_l^n} = \begin{cases} \dfrac{1}{E_i Z} + \dfrac{1}{E_j Z} & \text{Particle-Particle} \\ \dfrac{1}{E_i Z} + \dfrac{1}{E_w Z} & \text{Particle-Wall} \end{cases} \tag{7}$$

$$K_u^n = \frac{K_u^n}{\varepsilon^2} \tag{8}$$

Where $F_i^{n,T}$ and $F_i^{n,(T-\Delta T)}$ are the actual contact forces at time T and time T−ΔT, respectively, and ΔT is the time step. ΔS^n stands for normal overlapping variation, whereas $S^{n,T}$ and $S^{n,T-\Delta T}$ stand for normal overlap in the present and past, respectively. The unloading and loading contact stiffnesses are K_u^n and K_l^n, respectively, and the wall or boundary is w. ε is the restoration ratio, and Z is the particle size. E_i and E_w are the particle and boundary Young's moduli, respectively.

The Linear Spring Coulomb Limit Model (El-Emam et al., 2021) was used in this research to determine the total tangential contact force of the particle shear force during tangential contact (Equation 9).

$$F_i^{t,T} = min(F_i^{t,(T-\Delta T)} + K_l^n \Delta S^t, \mu F_i^{n,T}) \tag{9}$$

$F_i^{t,T}$ and $F_i^{t,(T-\Delta T)}$ are the tangentially contacting forces at the current and previous times, respectively, St is the change in tangential overlap throughout the time step, and is the friction coefficient indicating contact slip.

This numerical study used a one-way link between CFD and DEM, as well as an appropriate friction correlation model, to anticipate the actual behavior of the particulate matter flow in the cyclone separator (Peng et al., 2020; El-Emam et al., 2021).

The Ganser drag model (Ganser, 1993; Fonte et al., 2015; Almeida et al., 2016) has been successfully used since it is based on a single particle drag model. A discrete phase flow is a diluted flow whereby each particle is dealt with separately (El-Emam et al., 2021). Another strong reason to employ this model is that the particle matter in the simulation is non-spherical, having changing forms, densities, characteristics, alignment, and concentration. Therefore, the Ganser drag model can be accurately concluded using the particle relative Reynolds number and the two shape factors in the governing equations, as shown in (Equation. 10-13).

$$\frac{C_d}{K_2} = \frac{24}{R_{ep}K_1K_2}[1+0.1118(R_{ep}K_1K_2)^{0.6567}] + \frac{0.4305}{1+\frac{3305}{R_{ep}K_1K_2}} \tag{10}$$

$$K_1 = (\frac{d_p}{3d_v} + \frac{2}{3}\emptyset^{-0.5})^{-1} - 2.25\frac{d_v}{D} \tag{11}$$

$$K_2 = 10^{1.8148(-\log_{10}\emptyset)^{0.5743}} \tag{12}$$

$$R_{ep} = \frac{\rho_f|v_f - u_i|d_p}{\mu_f} \tag{1}$$

Where the coefficient of friction is Cd, the Reynolds number is R_{ep}, and the shape factors are Stokes and Newton, respectively. d_p is the diameter of a spherical particle whose reflected area is equal to the reflected area of the real particle. The particle's sphericity is $\emptyset$, the diameter of a solid sphere with the same volume as the real particle is d_v, the fluid viscosity is μ_f, and the particle diameter is D.

Numerical simulations were run in CFD ANSYS-Release-19 on a machine with an Intel(R) 2.10 GHz CPU and 16GB of RAM for this work, as well as in ROCKY DEM software, which was provided with a 6-month trial version. Here, the unidirectional coupling of the CFD-DEM is used since the movement of particles is only affected by the airflow (dilute flow), and the particle velocity at the inlet of the cyclone is considered to be the same as that of the surrounding air (Elghobashi, 1994; Elsayed and Lacor, 2014; El-Emam et al., 2021). It is also recommended for the simulation of large particles in one-way coupling and unlimited homogeneous flows with different particle densities (Elsayed and Lacor, 2011; Fonte et al., 2015; Almeida et al., 2016). The general view of the cyclone used in this study is given in Figure 2, and its dimensions are given in Table 1 The cut-off size of this cyclone was not determined in this study because the basic working principle of the cyclone in this study is that it will be used for packing or bagging the straw by separating the air from it.

Table 1. Dimensions of thedesign componentse

Companent	Geometry	Dimensions (mm)
Cyclone diameter	Dc	320
Cylinder length	Lc	420
Cone length	Zc	950
Vortex diameter	Dv	120
Vortex length	Lv	130
Straw outlet duct	Do	100
Straw and air intake duct	Di	100

First, three-dimensional unstructured networks (Slacket al., 2000; Chu et al., 2011) were arranged on the designed cyclone (Fig. 2). The goal here is to resolution-independent is network resolution independent. It has been found that the solution has changed with the network improvements made in the cyclone. This indicates that a network-independent solution has yet to be found. As a result, network enhancements were made, and the process was repeated until the solution remained unchanged as the network changed. The y+ value was assumed to be between 30 and 100 for these operations (El-Emam et al., 2021). The cyclone mesh network has a total of 98.255 cells. The CFD solution was then transferred to DEM to execute the CFD-DEM merger simulation after network independence was established.

In CFD simulations, the liquid film flow (air) conditions were used (El-Emam et al., 2021). The air characteristics in the cyclone were modified to be turbulent, with a temperature of 25°C, a density of 1,225 kg/m^3, and kinematic viscosity of 1.7894 106 kgm/s. To show the impacts of airflow, the RSM turbulence model is combined with typical wall functions. For each calculation model, the y+ value is between 30-100. This shows that the nodes closer to the wall are in the log-log layer and not in the laminar substrate (El-Emam et al., 2021). The terminal velocity for wheat straw varies between 4.80-6 m/s (Khoshtaghaza and Mehdizadeh, 2006). In this study, straw and air intake velocities were applied as 18-15-12-10-8-6-4 m s^{-1} inside the cyclone. Each velocity application has been tested at 100 g/s and 200 g/s straw inlet feed densities. Thus, a total of 200 g and 400 g straws have been entered at the cyclone input for each velocity value application. The DEM simulation values for the straw are given in Table 2. A straw particle of the same size was used to get a faster and more accurate result of the simulation time.

Table 2. DEM simulation values of straw

| Property	Unit	Straw
Particle Shape	-	Straight fiber
Dimensions	mm	5 (Equivelant diameter) x 20
Density	kg/m^3	200 (O'dogherty et al., 1995; Annoussamy et al., 2000)
Number of particles	-	18000
Coefficient of friction (straw-straw)	-	0.3 (Sitkei, 1987)
Coefficient of friction (straw-steel)	-	0.8 (Liu et al., 2018)
Coefficient of restitution		0.2 (Li et al., 2018)
Rolling resistance		0.3
Poisson's ratio		0.4 (Li et al., 2012; Liu et al., 2018)
Shear modulus of straw	GPa	0.001 (Liu et al., 2018)
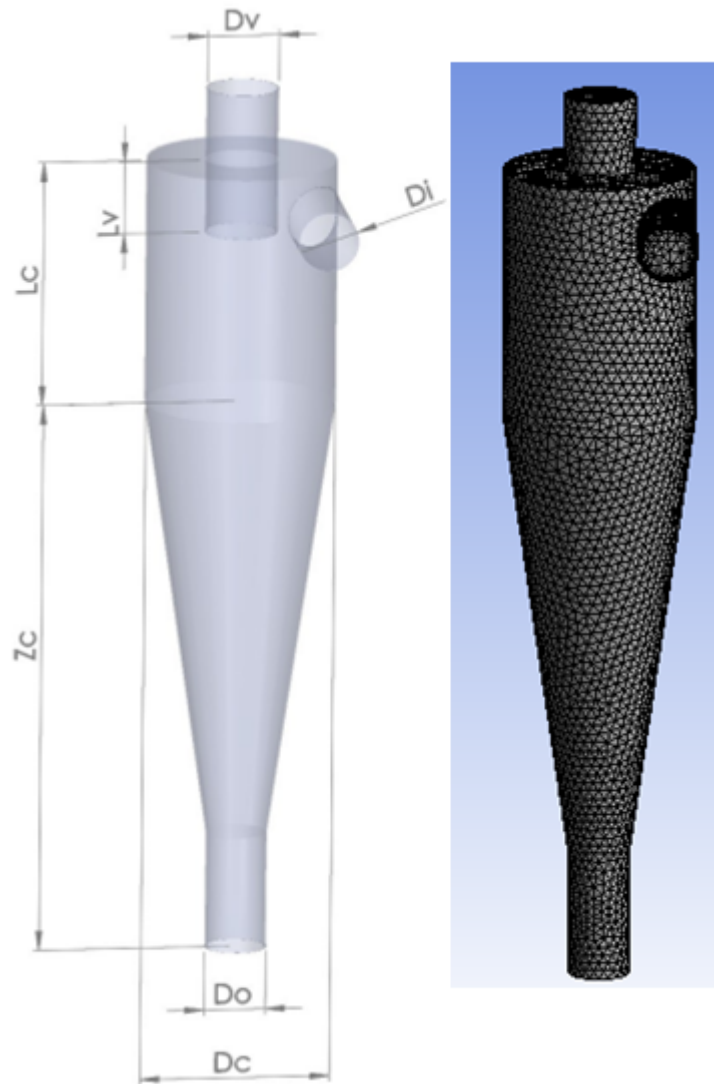
Figure 2. Cyclone model and mesh network.

One-way CFD-DEM coupling simulation was performed for each velocity value. A total of 14 different simulations were run, including air velocities and different feed densities. For each operating case, particulate matter was given proportionately to the air velocity at the inlet of the cyclone. The total simulation time was selected as 6 seconds before starting the simulations. The airflow was operated until the conclusion of the simulation period, while the cyclone was fed constantly till the 2nd second of the simulation time. Cube was made using the Processes component of Rocky's Particle program. With this Cube feature, the inlet and outlet mass values of the cyclone from both the inlet channel (Di) and the outlet channel (Do) of the straw to the straw are graphically and numerically taken with 0.1 second intervals from the first moment of the straw starting the flow (0th second) to the 6th second. Calculations under these conditions took approximately 40 to 60 hours, depending on each velocity value.

The output efficiency (s) was obtained in this study to evaluate the cyclone efficiency. The output efficiency (Equation 14) was computed by comparing the number of straws at the cyclone intake (feed) to the number of straws at the outflow (product) (Vose, 1978; Farran and Macmillan, 1979; Stepanenko, 2017; El-Emam et al., 2021).

$$\eta_s = \frac{\text{The amount of straw entering the cyclone}}{\text{The amount of straw coming out of the cyclone}} \times 100 \qquad (14)$$

3. Results and Discussion

Due to severe turbulence and violent vortex, cyclone separators have a complicated velocity profile at high air intake velocities. The findings of the CFD simulations looked at in this study were compared to varied velocities and velocity variations along the cyclone borders. To acquire an exact result of extraction efficiency and to depict the rotational properties of the airflow, a precise estimate of velocity variation levels is necessary. The Rankine vortex type is defined by the velocity profile that forms the typical flow shape (Peng et al., 2002; Cortes and Gil, 2007; Kozołub et al., 2017). The flow within reverse flow cyclone separators must follow this flow arrangement (Figure 3). On the outside, there is a free vortex, and in the middle, there is a forced vortex. The hay is forced out by the flow towards the cyclone barriers. The fluid flow direction in the core part of the cone section is inverted upwards, directed from the vortex finder to the cyclone exit. Figure 3 depicts the velocity profiles for the cyclone's various air input velocities.
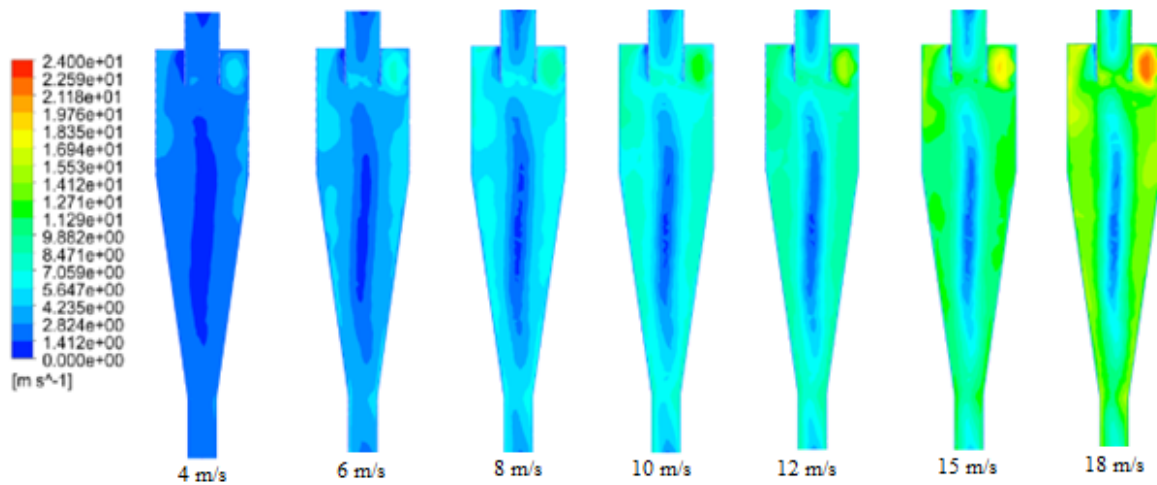

Figure 3. Velocity profiles in the cyclone of different inlet velocities.

In all of the different velocity combinations, the sidewalls of the cyclone had higher velocities than the center. The pressure distribution depending on the velocity profiles within the cyclone is shown in Figure 4. Positive high-pressure is seen at the entrance of the cyclone and on the side walls (cylinder (Lc) walls). This might imply that the wind in this location will have a greater influence on the straw particons than in others. While the pressure decreases in the middle of each cyclone, the pressure becomes negative at the vortex outlet (Dv). The streamline reverses its path towards the center of the cyclone near the end of the negative pressure zone, and air exits the cyclone through the vortex outlet. This situation is seen in Figure 4. The pressure on the sidewalls of the cyclone also increased due to the increase in air entry velocity into the cyclone. The flow near the cyclone walls is intended to push heavy particles towards the lower outlet end of the cyclone.
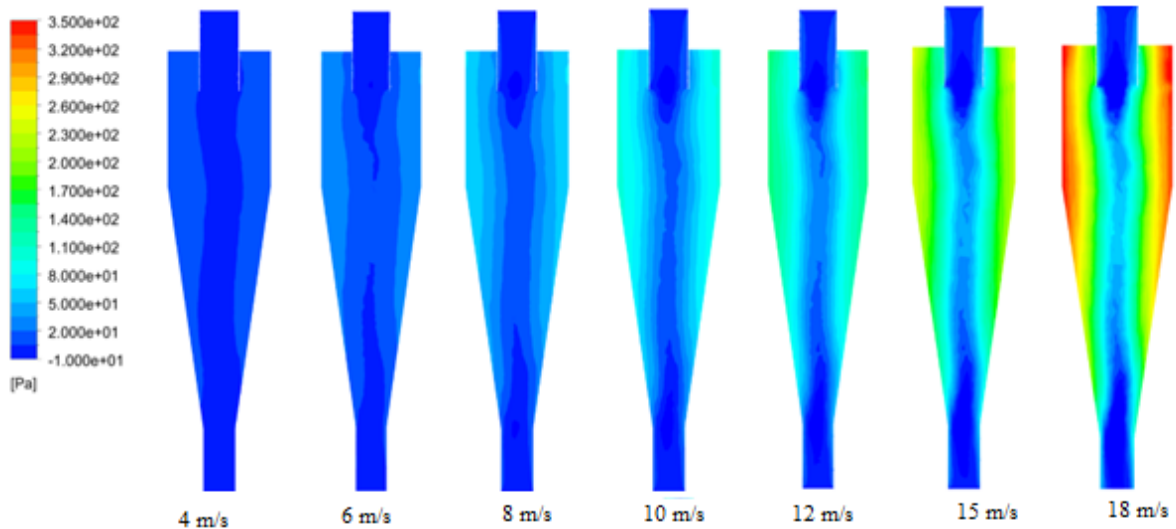
Figure. 4. Pressure distributions in the cyclone of different inlet velocities.

It is known that the majority of flow particles accumulate on the cyclone intake wall shortly after entering and then drop in strips (Wang et al., 2006; Li et al., 2009). As seen in Figures 5-6 and 7, particle behavior can be accurately captured by the current CFD-DEM model. It is seen that the flow reaches a steady state after 2 seconds, which is consistent with the literature (Chu et al., 2011).

The separation efficiency found in the cyclone is reflected in the spiral flow pattern of the straw. Particle flow usually enters the perimeter from the cyclone intake, and spirals are created around the barrel portion towards the top of the cyclone, as images of the simulation result from different time steps plainly demonstrate. They flow tangentially down to the conical section of the cyclone, generating an outer vortex. The higher air velocity in the outer vortex of the barrel section causes the heavier particles (straws) to be separated from the flow stream and gathered towards the cyclone wall due to increased centrifugal force. When the flow reaches the conical part, the air velocity drops drastically and creates an internal vortex. During this process, the straw fall from the end of the conical section as the airflow escapes the vortex finder. The flow of straw in the cyclone at rates of 4 m/s, 10 m/s, and 18 m/s is given as an example in Figure 5-6 and 7, respectively. It is seen that the straw moves from the cyclone walls to the straw outlet channel with the effect of the pressure on the cyclone wall. Similar relationships were also seen in other velocity trials and feeding values.

The time-dependent changes in the amount of straw particles coming out of the cyclone were examined at each velocity value. The output amounts of the straw particles were observed at a rate of at least 18 m/s at both 100 g/s (Figure 8) and 200 g/s (Figure 9) feed densities. The high velocity value prolonged the residence time of the straw in the cyclone and caused it to leave the cyclone later. With the increase in the cyclone inlet velocity, the straw output decreased at different simulation times due to the increase in the centrifugal force acting on the straw and the increase in the number of eddy rotations (Karpov and Saburov, 1998; Fıçıcı, 2006). This was particularly evident at the cyclone input velocities of 15 m/s and 18 m/s. The decrease in time-related product output at high air and hay input velocities was caused by the increase in the length of time the straw remained in the cyclone. Researchers have reported that gas velocity, particle inlet density, and particle diameter have increased particle residence time (Dibb and Silva, 1997; Corrêa et al., 2004; Corrêa et al., 2004; Farias et al., 2013). Corrêa et al. (2004a) study foundthe that if cyclone air flow rate increases from 8.6 kg/s to 9.25 kg/s, the residence time of the particle in the cyclone increases from 0.67 s to 1.27 s.

When we examine the Figures, it can be seen that many straws reach a steady state at the base of thclone in the 2.1 the second of the simulation period. However, it is seen that the straw flow at the highest velocity of 18 m/s is more unstable than the straw flow at the lower velocity values. We can explain the reason for this as the turbulent flow that occurs in the cyclone at high velocity.
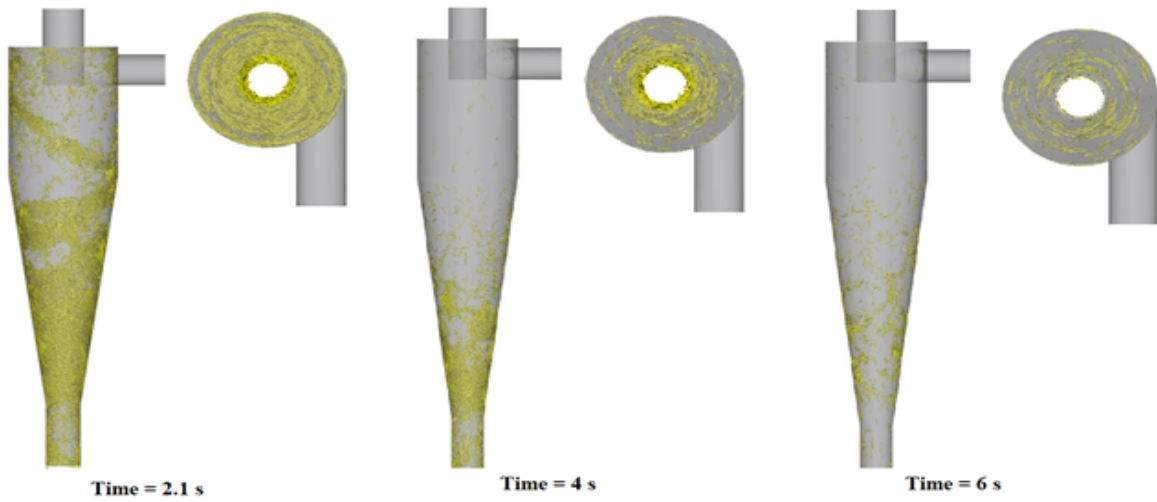
Figure 5. Time-dependent movement of straw in the cyclone at an inlet velocity of 4 m/s.
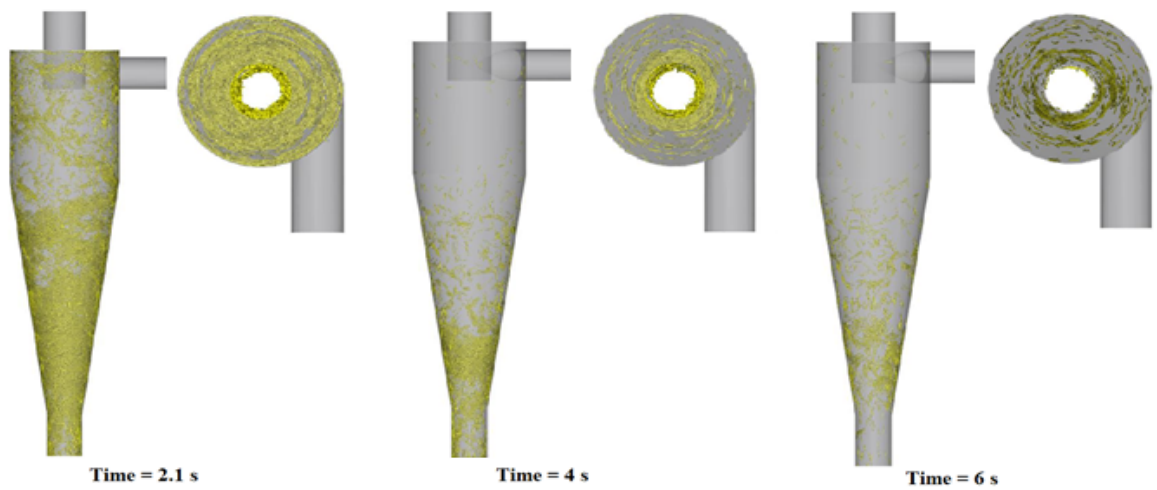

Figure 6. Time-dependent movement of straw in the cyclone at an inlet velocity of 10 m/s.
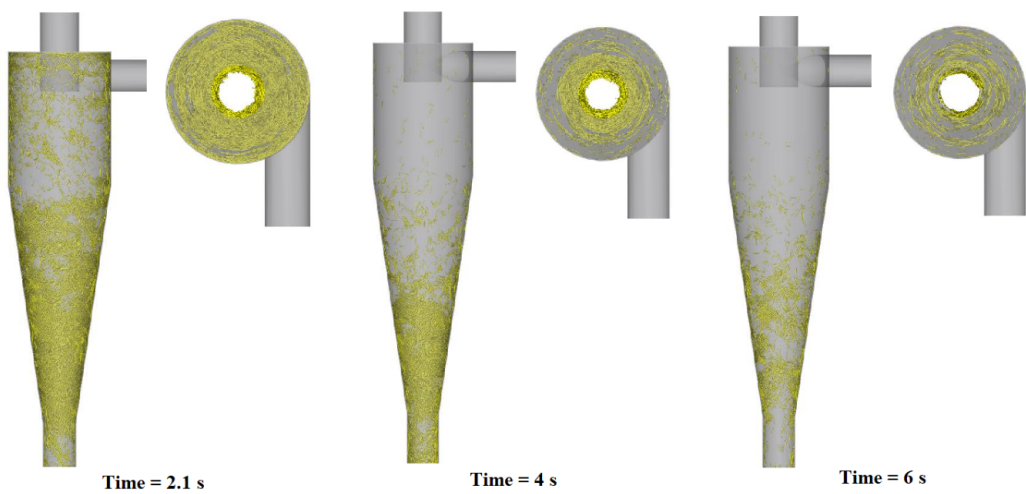

Figure 7. Time-dependent movement of straw in the cyclone at an inlet velocity of 18 m/s.
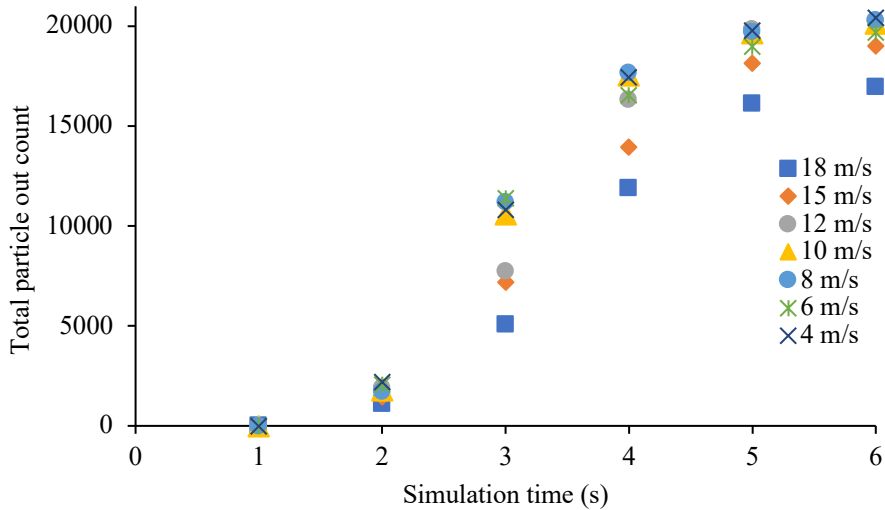
Figure 8. Total particle output amount of different velocities (at 100 g/s feed density).

The output efficiency at the end of the 6th second of the simulation was investigated at different air and straw inlet velocities and different straw inlet dinties into the cyclone (Figure 9). Output efficiency of both 100 g/s and 200 g/s straw inlet densities decreased at high inlet rates of 15 m/s and 18 m/. The highest output efficiency at 100 g/s and 200 g/s inlet densities were calculated as 93.8% and 96.4% at 12 m/s air inlet velocity, respectively. At low flow rates, the centrifugal force is weak, making regular flows of particles difficult. As a result, the output efficiency may be lower. At higher flow rates, however, the centrifugal force is strong, and the turbulent kinetic energy increases. This also affects the stability of the cyclone inflow field. This effect will intensify the back-mixing of particles and cause a reduction in output efficiency. In this study, there was a decrease in cyclone output efficiency at very low velocity and very high velocity. Ma et al. (2015) reported that in their three different cyclone designs and different flow rates (30-40-50-60-70 m³/h), they achieved the highest output efficiency of 50 m³/h flow rate. They reported reduced output efficiency at very low and very high flow rates in each cyclone model.

The increased feed density in the cyclone at the same air inlet rates has increased the hay output efficiency. Lim et al. (2003) reported that increased particle inlet density increases cyclone yield. Huang et al. (2018) explained in their study results that increasing particle mass loading improves separation efficiency. The separation efficiency is proportional to the residence time of the straw particle in the cyclone.
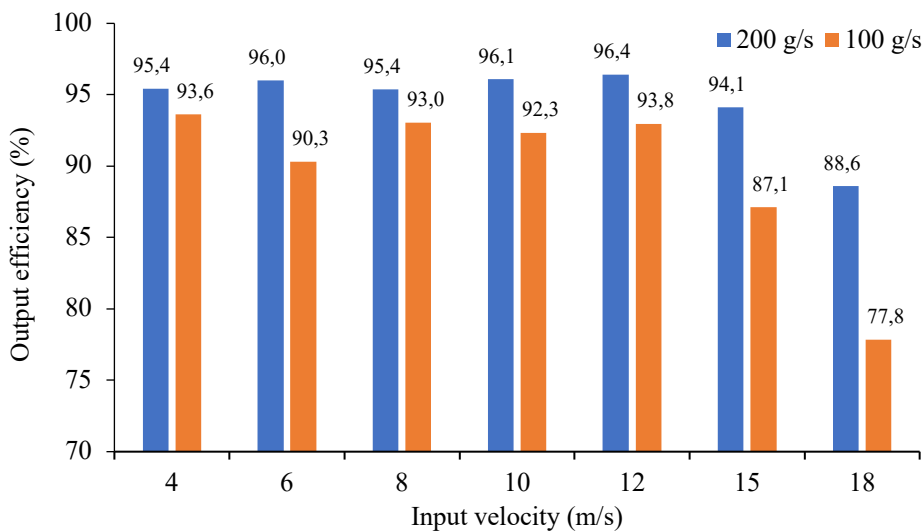

Figure 9. Cyclone output efficiency at different inlet velocities and feed densities.

4. Conclusion

The amount of straw particles exiting the cyclone was analyzed in a time-dependent manner in this study using CFD and DEM methods in a designed cyclone.

Reynolds stress turbulence model was used since the cyclone has a complex turbulent flow type as its flow type. During the simulation, the drag model caused the straws to form trajectories towards the bottom of the cyclone. According to the simulation results, there was an increase in pressure on the side walls of the cyclone due to the increase in the air inlet velocity to the cyclone. The flow near the cyclone walls caused the straw particles to be directed towards the lower exit end of the cyclone. At feed densities of 100 g/s and 200 g/s, the least particle output was obtained at a rate of 18 m/s. The high velocity value extended the residence time of the straw in the cyclone and delayed the separation of the straw from the cyclone. The highest cyclone output efficiency was obtained at feed densities of 100 g/s and 200 g/s at a velocity of 12 m/s. In addition, the increase in feeding density at constant air inlet velocity entering the cyclone increased the straw output efficiency. The simulation analysis results of the straw flow in the cyclone were found to be compatible with the literature. Thus, straw bagging or packaging will also guide in terms of improving the designs by using CFD and DEM simulation methods before cyclone designs. This research was the first attempt to model the airflow of straw particles using a cyclone separator.

References

Almeida, E., Spogis, N., & Silva, M. (2016). *Computational study of the pneumatic separation of sugarcane bagasse.* Paper presented at the Proceedings of the 6th International Conference on Engineering for Waste and Biomass Valorisation, Albi, France.

Annoussamy, M., Richard, G., Recous, S., & Guerif, J. (2000). Change in mechanical properties of wheat straw due to decomposition and moisture. *Applied Eng. in Agri., 16*(6), 657. doi:https://doi.org/https://doi.org/10.13031/2013.5366

Avcı, A., & Erel, G. (2003). Effect of Length on Production in Cyclone Separators and Optimization. *Uludağ University Journal of The Faculty of Engineering, 8*(1), 101-109.

Chu, K., Wang, B., Xu, D., Chen, Y., & Yu, A. (2011). CFD–DEM simulation of the gas–solid flow in a cyclone separator. *Chemical Eng. Sci., 66*(5), 834-847. doi:https://doi.org/10.1016/j.ces.2010.11.026

Corrêa, J., Graminho, D., Silva, M., & Nebra, S. (2004). The cyclonic dryer: a numerical and experimental analysis of the influence of geometry on average particle residence time. *Brazilian Jour. of Che. Engi., 21*(1), 103-112.

Corrêa, J. L., Graminho, D. R., Silva, M. A., & Nebra, S. A. (2004). Cyclone as a sugar cane bagasse dryer. *Brazilian Jour. of Che. Engi., 12*(6), 826-830.

Cortes, C., & Gil, A. (2007). Modeling the gas and particle flow inside cyclone separators. *Prog. in Energ. and Com. Sci., 33*(5), 409-452. doi:https://doi.org/10.1016/j.pecs.2007.02.001

Cundall, P. A., & Strack, O. D. (1979). A discrete numerical model for granular assemblies. *geotechnique, 29*(1), 47-65.

Dibb, A., & Silva, M. (1997). *Cyclone as a dryer–the optimum geometry.* Paper presented at the Proceedings of the First Inter-American Drying Conference (IADC).

Drew, D. A. (1983). Mathematical modeling of two-phase flow. *Annual review of fluid mechanics, 15*(1), 261-291.

El-Emam, M. A., Zhou, L., Shi, W., & Han, C. (2021). Performance evaluation of standard cyclone separators by using CFD–DEM simulation with realistic bio-particulate matter. *Pow. Tech., 385*, 357-374. doi:https://doi.org/10.1016/j.powtec.2021.03.006

Elghobashi, S. (1994). On predicting particle-laden turbulent flows. *Applied scientific research, 52*(4), 309-329.

Elsayed, K., & Lacor, C. (2011). The effect of cyclone inlet dimensions on the flow pattern and performance. *Appli. Mat. Model., 35*(4), 1952-1968. doi:https://doi.org/10.1016/j.apm.2010.11.007

Elsayed, K., & Lacor, C. (2014). Analysis and optimisation of cyclone separators geometry using RANS and LES methodologies. In *Turbul. and Interac.* (pp. 65-74): Springer.

Farias Neto, S. R., Farias, F. P. M., Delgado, J. M. P. Q., Lima, A. G., & Cunha, A. L. (2013). Cyclone: Their characteristics and drying technological applications. In *Industrial and Technological Applications of Transport in Porous Materials* (pp. 1-36): Springer.

Farran, I., & Macmillan, R. (1979). Grain-chaff separation in a vertical air stream. *Journal of Agr. Engi. Res., 24*(2), 115-129.

Faulkner, W. B., & Shaw, B. W. (2006). Efficiency And Pressure Drop Of Cyclones Across A Range Of Inlet Velocities. *Appli. Eng. in Agr., 22*(1), 155-161. doi:https://doi.org/10.13031/2013.20191

Fıçıcı, F. (2006). *An Experimental Investigation on The Effect of Plungİng Pipe Diameter Change in Cyclones to The Flow Parameters* (Master). Sakarya University, Sakarya.

Fluent, A. (2009). Ansys Fluent 12.0 Theory Guide. *ANSYS Inc., Canonsburg, PA*.

Fonte, C. B., Oliveira Jr, J. A., & de ALMEIDA, L. C. (2015). *DEM-CFD coupling: mathematical modelling and case studies using ROCKY-DEM® and ANSYS Fluent®.* Paper presented at the Proceedings of the 11th International Conference on CFD in the Minerals and Process Industries, CSIRO, Melbourne, Australia.

Freireich, B., Litster, J., & Wassgren, C. (2009). Using the discrete element method to predict collision-scale behavior: a sensitivity analysis. *Chemi. Eng. Sci., 64*(15), 3407-3416. doi:https://doi.org/10.1016/j.ces.2009.04.019

Ganser, G. H. (1993). A rational approach to drag prediction of spherical and nonspherical particles. *Pow. Techn., 77*(2), 143-152. doi:https://doi.org/10.1016/0032-5910(93)80051-B

Gimbun, J., Chuah, T., Fakhru'l-Razi, A., & Choong, T. S. (2005). The influence of temperature and inlet velocity on cyclone pressure drop: a CFD study. *Chemi. Eng. and Proces. :Pro. Intensifi., 44*(1), 7-12. doi:https://doi.org/10.1016/j.cep.2004.03.005

Gronald, G., & Derksen, J. (2011). Simulating turbulent swirling flow in a gas cyclone: A comparison of various modeling approaches. *Pow. Tech., 205*(1-3), 160-171.

He, Y., Bayly, A. E., & Hassanpour, A. (2018). Coupling CFD-DEM with dynamic meshing: A new approach for fluid-structure interaction in particle-fluid flows. *Pow. Tech., 325*, 620-631. doi:https://doi.org/10.1016/j.powtec.2017.11.045

Huang, A.-N., Ito, K., Fukasawa, T., Fukui, K., & Kuo, H.-P. (2018). Effects of particle mass loading on the hydrodynamics and separation efficiency of a cyclone separator. *Jour. of the Taiw. Inst. of Chem. Eng., 90*, 61-67. doi:https://doi.org/10.1016/j.jtice.2017.12.016

Jakirlic, S., Hanjalic, K., & Tropea, C. (2002). Modeling rotating and swirling turbulent flows: a perpetual challenge. *AIAA journal, 40*(10), 1984-1996. doi:https://doi.org/10.2514/2.1560

Karpov, S., & Saburov, E. (1998). Optimization of geometric parameters for cyclone separators. *Theor. Foun. of Chem. Eng., 32*(1), 7-12.

Khoshtaghaza, M., & Mehdizadeh, R. (2006). Aerodynamic properties of wheat kernel and straw materials. *Agr. Eng. Intern.: CIGR Jour.*

Kozołub, P., Klimanek, A., Białecki, R. A., & Adamczyk, W. P. (2017). Numerical simulation of a dense solid particle flow inside a cyclone separator using the hybrid Euler–Lagrange approach. *Particuol., 31*, 170-180. doi:https://doi.org/10.1016/j.partic.2016.09.003

Li, H., Li, Y., Gao, F., Zhao, Z., & Xu, L. (2012). CFD–DEM simulation of material motion in air-and-screen cleaning device. *Comp. and Electr. in Agr., 88*, 111-119. doi:https://doi.org/10.1016/j.compag.2012.07.006

Li, S., Yang, H., Zhang, H., Yang, S., Lu, J., & Yue, G. (2009). Measurements of solid concentration and particle velocity distributions near the wall of a cyclone. *Chem. Eng. Jour., 150*(1), 168-173. doi:https://doi.org/10.1016/j.cej.2008.12.019

Lim, K., Kwon, S., & Lee, K. (2003). Characteristics of the collection efficiency for a double inlet cyclone with clean air. *Jour. of Aerosol Sci., 34*(8), 1085-1095. doi:https://doi.org/10.1016/S0021-8502(03)00079-X

Liu, F., Zhang, J., & Chen, J. (2018). Modeling of flexible wheat straw by discrete element method and its parameter calibration. *Inter. Jour. of Agri.. and Biologi. Eng., 11*(3), 42-46. doi:DOI: 10.25165/j.ijabe.20181103.3381

Ma, L., Fu, P., Wu, J., Wang, F., Li, J., Shen, Q., & Wang, H. (2015). CFD simulation study on particle arrangements at the entrance to a swirling flow field for improving the separation efficiency of

cyclones. *Aerosol and Air Qual. Res., 15*(6), 2456-2465. doi:https://doi.org/10.4209/aaqr.2015.02.0126

Marinuc, M., & Rus, F. (2011). The effect of particle size and input velocity on cyclone separation process. *Bulletin of the Transilvania University of Brasov. Forestry, Wood Industry, Agricultural Food Engineering. Series II, 4*(2), 117.

Neuwirth, J., Antonyuk, S., Heinrich, S., & Jacob, M. (2013). CFD–DEM study and direct measurement of the granular flow in a rotor granulator. *Chemi. Eng. Sci., 86*, 151-163. doi:https://doi.org/10.1016/j.ces.2012.07.005

O'dogherty, M., Huber, J., Dyson, J., & Marshall, C. (1995). A study of the physical and mechanical properties of wheat straw. *Jour. of Agri. Eng. Res., 62*(2), 133-142. doi:https://doi.org/10.1006/jaer.1995.1072

Peng, G., Huang, X., Zhou, L., Zhou, G., & Zhou, H. (2020). Solid-liquid two-phase flow and wear analysis in a large-scale centrifugal slurry pump. *Engin. Fail. Analy., 114*, 104602. doi:https://doi.org/10.1016/j.engfailanal.2020.104602

Peng, W., Hoffmann, A., Boot, P., Udding, A., Dries, H., Ekker, A., & Kater, J. (2002). Flow pattern in reverse-flow centrifugal separators. *Pow. Tech., 127*(3), 212-222. doi:https://doi.org/10.1016/S0032-5910(02)00148-1

Rocky, E. (2018). Rocky DEM technical manual.

Sitkei, G. (1987). *Mechanics of agricultural materials*: Elsevier.

Slack, M., Prasad, R., Bakker, A., & Boysan, F. (2000). Advances in cyclone modelling using unstructured grids. *Chem. Engi. Res. and Des., 8*(78), 1098-1104. doi:https://doi.org/10.1205/026387600528373

Stepanenko, S. (2017). *Research pneumatic gravity separation grain materials.* Paper presented at the Scientific Proceedings V International Scientific-Technical Conference "Agricultural Machinery" 2017.

Şendoğan, Ö. (2012). *Desin of High Efficient Cyclone and Experimental Investigation Its Performance* (MSc Thesis). Uludağ University,

Vose, J. (1978). Separating grain components by air classification. *Separation and Purification Methods, 7*(1), 1-29.

Walton, O. R., & Braun, R. L. (1986). Viscosity, granular-temperature, and stress calculations for shearing assemblies of inelastic, frictional disks. *Journal of rheology, 30*(5), 949-980.

Wan, G., Sun, G., Xue, X., & Shi, M. (2008). Solids concentration simulation of different size particles in a cyclone separator. *Pow. Tech., 183*(1), 94-104. doi:https://doi.org/10.1016/j.powtec.2007.11.019

Wang, B., Xu, D., Chu, K., & Yu, A. (2006). Numerical study of gas–solid flow in a cyclone separator. *Appli. Math. Model., 30*(11), 1326-1342. doi:https://doi.org/10.1016/j.apm.2006.03.011

Wang, L., Parnell, C. B., & Shaw, B. W. (2002). A study of the cyclone fractional efficiency curves. *Intern.. Comm. of Agri. Engi., 4*. doi:https://hdl.handle.net/1813/10270

Xiang, R., & Lee, K. (2005). Numerical study of flow field in cyclones of different height. *Chem. Engin. and Proces.: Proc. Inten., 44*(8), 877-883. doi:https://doi.org/10.1016/j.cep.2004.09.006

Zhou, L., Han, C., Bai, L., Li, W., El-Emam, M. A., & Shi, W. (2020). CFD-DEM bidirectional coupling simulation and experimental investigation of particle ejections and energy conversion in a spouted bed. *Energ., 211*, 118672. doi:https://doi.org/10.1016/j.energy.2020.118672

Zhu, H., Zhou, Z., Yang, R., & Yu, A. (2008). Discrete particle simulation of particulate systems: a review of major applications and findings. *Chem. Engin. Sci., 63*(23), 5728-5770. doi:https://doi.org/10.1016/j.ces.2008.08.006